41st AIAA Fluid Dynamics Conference AIAA-2011-3717
27 – 30 Jun 2011, Honolulu, HI

Further Experiments on Temporal Proper Orthogonal Decomposition for Closed-Loop Flow Control

Stanislav Gordeyev[1], Lee Neuharth[2], Flint O. Thomas[3] and Michael Wicks[4]
Department of Aerospace & Mechanical Engineering, Notre Dame, IN, 46556

Motivated by closed-loop flow control applications, a formulation of the proper orthogonal decomposition (POD) is demonstrated which is capable of characterizing not only the controlled and natural states of a given flow, but also the transient behavior between these states. This approach, which is termed temporal POD (TPOD) extracts the optimum frame-of-reference and the temporal information regarding the dynamics of the system in the presence of the flow control. In this paper the TPOD approach is applied to two experiments using active flow control: (1) flow over a circular cylinder at subcritical Reynolds number and (2) flow over a NACA 0015 airfoil at a post-stall angle of attack. Both flows exhibit well-defined and distinct natural and controlled flow states. TPOD is shown to be a very effective tool in characterizing these two states as well as the system trajectories associated with the transient behavior in between.

Nomenclature

a_i	=	temporal coefficient of spatial-temporal eigenfunction
$c_{i,j}$	=	temporal coefficient of spatial eigenfunction
C	=	controlled flow state
$d_{i,j}$	=	temporal coefficients of spatial eigenfunction for a given realization
D	=	cylinder diameter
E	=	expected value
f	=	temporal frequency
i,j	=	mode indices
N	=	natural flow state
R	=	two-point cross-correlation function
u	=	instantaneous velocity field
x	=	streamwise spatial coordinate
y	=	cross-stream spatial coordinate
t	=	time
t_o	=	system trajectory initial condition
α	=	realization number
λ_i	=	i-mode eigenvalue
ϕ_i	=	spatial-temporal i-mode eigenfunction
$\psi_{i,j}$	=	spatial mode eigenfunction
τ	=	time-delay after initiation of flow control

[1] Research Associate Professor, Department of Mechanical and Aerospace Engineering, Hessert Laboratory for Aerospace Research, Notre Dame, IN 46556, Senior AIAA Member.
[2] Graduate Student, Department of Mechanical and Aerospace Engineering, Hessert Laboratory for Aerospace Research, Notre Dame, IN 46556.
[3] Professor, Department of Mechanical and Aerospace Engineering, Hessert Laboratory for Aerospace Research, Notre Dame, IN 46556, AIAA Associate Fellow.
[4] Graduate Student, Department of Mechanical and Aerospace Engineering, Hessert Laboratory for Aerospace Research, Notre Dame, IN 46556.

I. Introduction and Objectives

For application to closed-loop flow control, it is desirable to obtain a low-order model of the candidate flow field that satisfactorily captures the dynamics of both the natural and controlled states, as well as transient regimes between these states. It is well known that conventional proper orthogonal decomposition (POD)-based modeling extracts an optimal, complete set of dominant (in terms of energy) spatial modes, such that a minimum number of modes are required to represent a particular flow state [1-3]. The projection of these modes onto the governing Navier-Stokes (N-S) equations provides a low-dimensional system of ordinary differential equations that describe the temporal evolution of the modes [4,5]. It is clear that this approach can suffer if the flow field is manipulated by some form of flow control and the natural and controlled states of the flow are sufficiently dissimilar. This is because the set of POD modes that is optimal in describing the natural flow state may do a comparably poor job describing the forced or controlled flow state. In other words, when flow control is activated, the set of POD modes derived to describe the natural flow with as few eigenvectors as possible becomes quite non-optimal for the controlled flow, and, although the set of POD modes is still complete, it results in a dramatic increase in the number of POD modes needed to provide a proper frame of reference to describe the forced flow. This is not satisfactory for closed loop flow control applications. This problem has long been recognized and several modifications of the basic POD approach have been proposed to address this issue. For periodic flows, so-called double POD or DPOD [6,7] provides a set of POD modes calculated within each period, and then performs a second POD-optimization among POD modes between periods, thus providing the eigenvector basis to optimally describe the natural, the transient and the forced states. However, the method may not be readily extended to more general aperiodic flows. Split POD [8] provides an extended POD basis which is optimal for both the natural and the forced states, but may not be optimal for the transient state, thus potentially losing information regarding how the flow goes from the natural to the forced state and back. Balanced POD [9] was demonstrated to capture proper dynamical modes from the flow, but can be used only in computational studies, since it requires the solution of the adjoint problem, though a technique called Eigensystem Realization Algorithm [10] has recently shown some promise to calculate Balanced POD modes directly from experiments [11]. In [12] a new formulation of the POD was presented which is capable of characterizing not only the controlled and natural states of a given flow but also the transient behavior between these states. This approach, which is termed temporal POD (TPOD) extracts the optimum frame-of-reference and the temporal information regarding the dynamics of the system in the presence of the flow control. The technique was demonstrated experimentally in an application involving flow control of a circular cylinder in cross-flow at subcritical Reynolds numbers. Dielectric barrier discharge (DBD) plasma flow control was used as the means of active flow control. The resulting low-order dynamical system model was shown to properly capture the correct dynamics of the first TPOD mode, including the natural, forced and transient regimes.

This paper represents a natural extension of the work reported in [12]. Refined flow control experiments utilizing the new TPOD approach are presented for both a cylinder in cross flow at subcritical Reynolds number as well as a NACA 0015 airfoil with leading edge plasma separation control. The objective of the cylinder flow control work is to extend the results presented in [12] by controlling the phase of flow control initiation relative to the natural shedding cycle. This is followed by application of TPOD to leading edge flow control on an airfoil at a post-stall angle of attack. Prior to describing these new results, we review the basis aspects of the TPOD technique in the following section.

II. Brief Overview of the TPOD Approach

Consider a system which at any moment, t, is described by an instantaneous field or a trajectory, $u(x,y,t)_\alpha$, where α denotes a particular realization. The flow control is activated at time $t = t_0$, so the system is in the natural state $u^N(x,y,t)_\alpha$ for $t < t_0$ and is in the forced or controlled state $u^C(x,y,t)_\alpha$ for $t - t_0 \to \infty$. Realizing that the flow is not homogeneous in time after the flow control is applied, the instantaneous flow field can be written as a function of the time delay after the flow control is activated, $\tau = t - t_0$, as $u(x,y,\tau = t - t_0; t_0 \in \{t_0\}_a)$. This defines an instantaneous system trajectory as a function of space, the time delay and the initial moment the flow control is applied.

Temporal POD decomposes the system trajectories into a low-dimensional set using *spatial-temporal* orthogonal-in-space eigenmodes, $\{\varphi_i(x,y,\tau)\}$, which are calculated from the cross-correlating system trajectories over all initial times, $t_0 \in \{t_0\}_\alpha$, for a fixed time delay,

$$\int R(x,y;x',y';\tau)\phi_i(x',y';\tau)dx'dy' = \lambda_i(\tau)\phi_i(x,y;\tau), \quad (1)$$

where $R(x,y;x',y';\tau) = E\{u(x,y;\tau;\{t_0\}_a)\cdot u(x',y';\tau;\{t_0\}_a)\}_\alpha$. Each flow trajectory can be represented in the low-dimensional space spanned by eigenmodes as,

$$u(x,y;\tau,t_0) = \sum_i a_i(\tau,t_0)\phi_i(x,y;\tau), \quad (2)$$

and each temporal coefficient is calculated by projecting the instantaneous flow trajectory into a TPOD mode,

$$a_i(\tau;t_0) = \int u(x,y;\tau,t_0)\phi_i(x,y;\tau)dxdy, \quad (3)$$

Finally, $E\{a_i^2(\tau,t_0)\}_\alpha = \lambda_i(\tau)$ is the ensemble-averaged mode energy at a given time delay τ.

By construction, TPOD modes provide very important information about *how* the system travels from the natural to the controlled state. The low-dimensional representation of both the natural and controlled states can be recovered from these TPOD eigenmodes, as $\varphi_i^N(x,y) = \varphi_i(x,y,\tau \le 0)$ and $\varphi_i^C(x,y) = \varphi_i(x,y,\tau \to \infty)$, respectively. A schematic of the TPOD reconstruction of system trajectories is shown in Figure 1. For simplicity, both the natural and controlled states are graphically represented by limiting cycles. When the flow control is applied at $\tau = 0$, the flow leaves the natural state and approaches the controlled state. Individual trajectories depend on the time delay and the initial time, or the point where the trajectory departs the natural state. All initial times can be described by projecting the trajectories into TPOD modes in the natural state, $u(x,y;t_0) = \sum_i a_i(t_0)\phi_i^N(x,y)$. So, each initial time can be represented by the set of temporal coefficients, $\{a_i(t_0)\}_\alpha$. For every fixed time delay, flow realizations are decomposed into a set of spatial TPOD modes; the set parametrically depends on the time delay. Each trajectory is approximated by the low-dimensional set of TPOD modes and the topology of flow trajectories can be analyzed as a function of the initial time and the time delay.

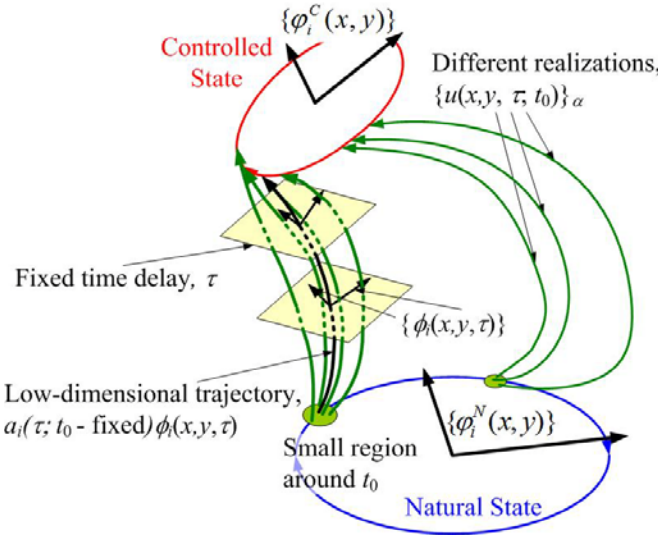

Figure 1. Topological definition of spatial TPOD modes.

It is convenient to project each deterministic *spatial-temporal* TPOD mode, $\phi_i(x,y,\tau)$ into a set of *spatial* modes, $\psi_{i,j}(x,y)$ using the traditional POD technique as,

$$\phi_i(x,y,\tau) = \sum_j c_{i,j}(\tau)\psi_{i,j}(x,y), \quad (4)$$

The set of $\Psi_{(i,j)}$-POD modes provides the optimal set of eigenvectors to describe the natural, transient and control states. The temporal coefficients, $c_{i,j}(\tau)$, define trajectories of the TPOD mode, $\varphi_i(x,y,\tau)$ in the Ψ-mode space; they provides an optimal way to store spatial-temporal TPOD modes. They can also be used to expand each individual trajectory as,

$$u(x,y;\tau,t_0) = \sum_i d_{i,j}(\tau,t_0)\Psi_{i,j}(x,y), \quad (5)$$

Another way to extract the flow trajectories is to combine the space and the time delay into a larger, spatial-temporal space, (x,y,τ), and compute a different set *spatial-temporal* TPOD modes as,

$\int R_{x,y,\tau}(x,y;x',y';\tau,\tau')\Phi_i(x',y';\tau')dx'dy'd\tau' = \Lambda_i\Phi_i(x,y;\tau)$, where

$R_{x,y,\tau}(x,y;x',y';\tau,\tau') = E\{u(x,y;\tau;\{t_0\}_a)\cdot u(x',y';\tau';\{t_0\}_a)\}_\alpha$. In this case, each flow trajectory can be represented as,

$$u(x,y;\tau,t_0) = \sum_i b_i(t_0)\Phi_i(x,y;\tau), \tag{6}$$

and each *b*-coefficient is calculated by projecting an instantaneous flow trajectory into a spatial-temporal mode, Φ_i, $b_i(t_0) = \int u(x,y;\tau,t_0)\Phi_i(x,y;\tau)dxdyd\tau$.

In general, each flow trajectory should be resolved both in space and time with good resolution. While, computationally this is generally not an issue, experimentally it might be a very challenging problem, as traditional particle image velocimetry (PIV) systems typically measure the velocity field with low sampling speeds. Emergence of the high-speed (up to a few kHz sampling rates) PIV systems with good spatial resolution promises to solve this problem. But, in some cases the information about flow trajectories still can be extracted using a traditional, low-speed PIV system. For instance, if the natural state is a limiting cycle, it is possible to perform conditional flow measurements and measure the flow dynamics for a subset of initial times originating from a small region in the natural state.

We will illustrate the TPOD technique by applying flow control for two candidate flows: one is the flow over a circular cylinder with the natural state a simple limiting cycle. The other is a more complex separated flow behind an airfoil. The next section describes the experimental apparatus and the two candidate flow fields utilized for demonstration of the TPOD technique. The results section will present experimentally-extracted TPOD modes for the cylinder flow using conditional sampling in conjunction with a low-speed PIV and for the airfoil flow using a high-speed PIV system.

III. Experimental Apparatus

All the experiments were performed in a low-turbulence, subsonic, in-draft wind tunnel located at the Hessert Laboratory for Aerospace Research at the University of Notre Dame. The wind tunnel has an inlet contraction ratio of 20:1. A series of 12 turbulence management screens at the front of the inlet give rise to tunnel freestream turbulence levels less than 0.1% (and less than 0.06% for frequencies above 10 Hz). Experiments are performed in a test section of 0.610 m square cross-section and 1.82 m in length. One sidewall and the ceiling have optical access for both flow visualization and PIV as nonintrusive laser flow-field diagnostics.

A. Description of Candidate Flow Fields for Application of TPOD

1) Circular Cylinder in Cross Flow

In [12] the TPOD approach was demonstrated in an experiment involving active control of flow over a circular cylinder at subcritical Reynolds number using dielectric barrier discharge (DBD) plasma actuators. Details of the experiment have been documented elsewhere [12, 13] so only essential aspects are described here. Twin spanwise-oriented DBD plasma actuators were mounted on the cylinder surface near $\pm 90^o$ (with respect to the oncoming flow) as shown schematically in Figure 2. The overall cylinder outer diameter was *D* =19 mm. The ends of the cylinder terminate in plastic endplates. The exposed and insulated electrodes are common for both of the plasma actuators due to space limitations. The reader unfamiliar with DBD plasma actuators is referred to recent comprehensive reviews of their application to aerodynamic flow control [14,15]. As indicated in the figure, the actuators are connected to a high voltage a.c. source that provides a 62kV peak-to-peak positive ramp waveform excitation to the electrodes at a frequency of 1 kHz. The plasma actuators produce quasi-steady plasma-induced wall jets on the cylinder surface that delay flow separation from the cylinder, which has been shown to have a dramatic effect on the cylinder wake with the elimination of unsteady Karman shedding. Consequently, the flow has two well defined states: the natural state which features unsteady Karman shedding of large-scale antisymmetric vortices into the wake and the plasma controlled state in which the separation region is greatly reduced in size and vortex shedding is totally suppressed. These two flow states are shown in Figure 3.

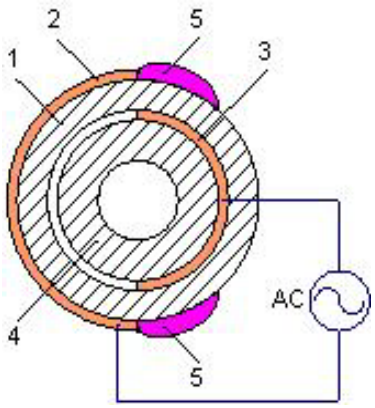

Figure 2. Schematic of the cylinder model equipped with spanwise-oriented plasma actuators: (1) quartz dielectric barrier, (2) surface electrode, (3) covered electrode, (4) internal insulation, (5) plasma discharge.

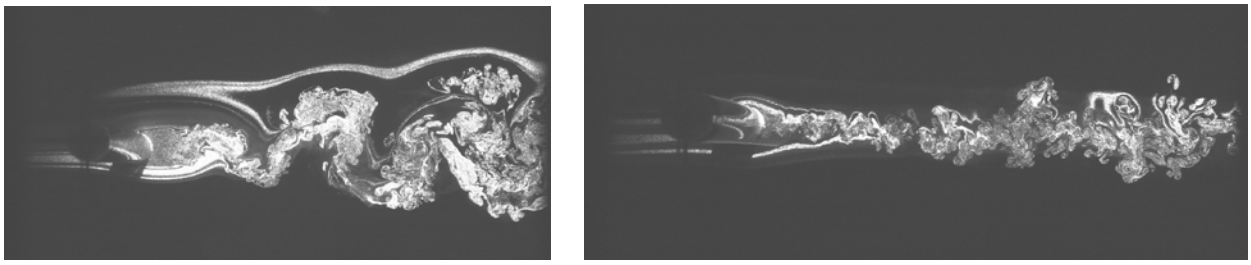

Figure 3. Flow visualization of Re_D = 5000 flow over the circular cylinder: (left) the natural state, (no plasma flow control) , (right) the controlled state (plasma on).

For the work reported in this paper, the plasma actuators on the cylinder were always operated in a quasi-steady mode in the sense that an unmodulated ac carrier of constant frequency was used when flow control was applied. The velocity data for the TPOD analysis were obtained non-intrusively using PIV measurements. The air upstream of the wind tunnel inlet was seeded with olive oil droplets of nominally 1 micrometer diameter that are produced by a TSI atomizer. A model Y120-15 New Wave Research Nd:Yag laser produced double laser pulses with a 25μs time interval. The maximum pulse repetition rate for this laser was 15 Hz. PIV images were captured by a PIV CAM 10-30 digital camera. TSI Insight 6 software was used to obtain a vector velocity field from each image pair. The interrogation region was approximately 6.5 cylinder diameters downstream of the end of the cylinder and 6.5 diameters in the cross-stream direction.

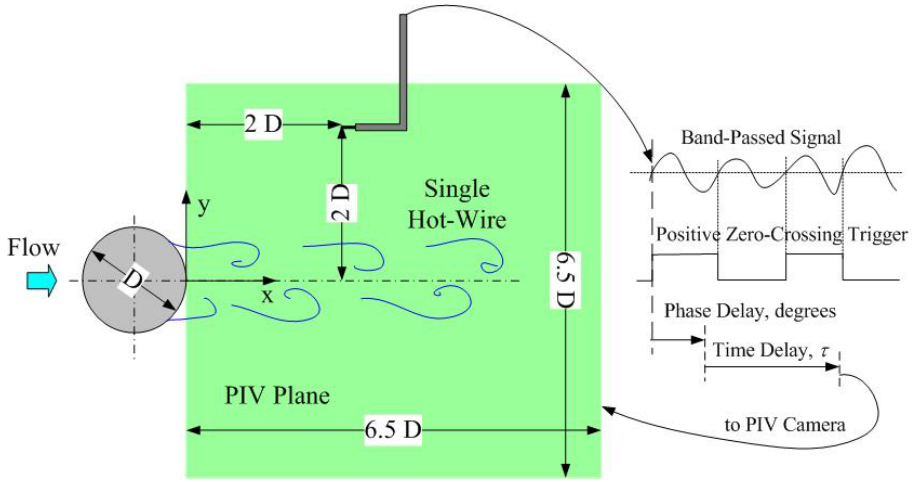

Figure **4. Schematic of experimental set-up with hot-wire signal as a trigger.**

The free stream velocity for the experiments was U_∞ = 4 m/s, which corresponds to a Reynolds number (based on cylinder diameter, *D*) of approximately Re_D = 5,000. The experiment consisted of multiple cycles of turning the twin DBD plasma actuators on and off. The plasma actuators were always operated in phase. Turning the plasma actuators on forced the flow from the natural to the controlled state and subsequently turning the plasma off allowed the flow to return to the natural state. In the experiments, the plasma was turned on for 125 msec and then turned off for 235 msec, so that the corresponding total plasma on-off cycle period was 360ms. The plasma on–off cycle was non-intrusively sampled via PIV with variable delay time steps, referenced from the initial moment, t_0, the plasma actuators were turned on. The resulting PIV data set was conditionally sampled to obtain 300 independent realizations for each fixed value of the time delay, τ.

To distinguish between different paths from the natural to the controlled state, the TPOD approach should be applied for different small regions of initial times. In the case of the natural time-periodic motion under consideration here, it is desirable to phase lock the initiation of plasma flow control relative to the cylinder's natural shedding cycle. By doing this, we phase-lock the trajectory to a small region in phase-space that takes the system from the natural to controlled state, as schematically shown in Figure 1. It should be noted that phase locking was not attempted in [12]. In order to achieve phase-lock, a single constant temperature hot wire probe was placed *x* =

2*D* downstream of the cylinder trailing edge, *y* = 2*D* above the cylinder axis and z = 0.4*D* spanwise offset between the probe and the PIV laser light sheet, as shown schematically in Figure 4. Although the hot-wire was outside the cylinder wake, it sensed the wake shedding state via Biot-Savart induction from large-scale wake vortices. The hot-wire velocity signal was filtered in a band centered on Strouhal shedding frequency of $f \approx 42$ Hz and was a.c.-coupled. Eight phase reference points were assigned to a hot-wire positive zero-crossing with a voltage comparator circuit, see Figure 4. A fixed phase delay was added to the phase reference point to define different and distinct phase-locked state (i.e. to specify a subset of t_o) and the PIV camera was triggered after a given time delay from this phase delay, as shown in Figure 4. In this manner, multiple flow field realizations could be acquired for plasma initiated at a selected phase (t_o) of the natural shedding cycle and at the desired time-delay, τ, relative to plasma initiation.

2) NACA 0015 Airfoil in Post-Stall Configuration

The second application of the TPOD method involves active leading edge flow control of a NACA 0015 airfoil in a static post-stall configuration. Flow control consisted of dielectric barrier discharge (DBD) plasma actuation applied to the airfoil leading edge.

The airfoil model is shown schematically in Figure 5. It was cast from a two-piece, CNC-machined aluminum mold with an epoxy-based polymer containing glass microspheres. The airfoil chord length was 127 mm. Two Plexiglas endplates were fastened to the edges of the airfoil in order to minimize 3-D effects. An internal cavity at the leading edge was flush-fitted with a DBD plasma actuator. As indicated in Figure 5, the covered electrode (1) and exposed electrode (3) were made from Saint Gobain C661, 0.0254 mm-thick copper foil tape with acrylic adhesive. The dielectric barrier (2) consists of a 5 mm layer of Kapton tape and a 1 mm layer of Teflon tape. Constructing the actuator in this manner allowed for precise placement of the electrode overlap so that plasma (4) would form on the leading edge before the onset of flow separation. Also, it provided a hydrodynamically-smooth leading edge, so as not to trip the flow. A high voltage a.c. power source provides a 10kV peak-to-peak positive ramp waveform at a carrier frequency of 2.3 kHz utilizing the circuit discussed in [16]. The plasma actuation in this case was unsteady and was pulsed at 2.5 Hz. The duty cycle was 25%. The freestream velocity was U_∞ = 10 m/s which corresponds to a chord Reynolds number of $Re_C \approx 86{,}000$. The airfoil was fixed at the post-stall angle of attack of $\alpha = 18^o$; the static stall angle is approximately $\alpha_s = 9^o$.

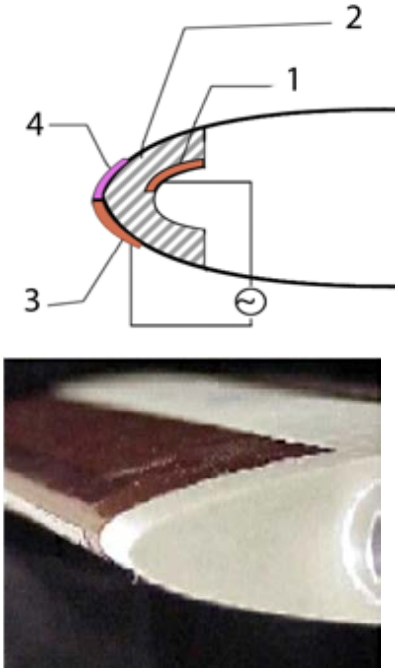

Figure 5: (top) Schematic of plasma actuator on airfoil model, (bottom) Picture of the airfoil leading edge.

High-speed PIV measurements were used to non-intrusively acquire velocity data. A TSI atomizer produced nominally one-micron diameter DEHS seed particles injected upstream of the wind tunnel inlet. A Litron LDY300 series Nd:YLF pulse laser and a Photron SA 1.1 high-speed camera were operated in double-frame mode with $\Delta t = 1000\ \mu s$ to capture images of the flow field, so the velocity field was acquired at a sampling rate of 1 kHz. The interrogation region was approximately 640 x 304 pixels corresponding to a physical domain of 275.1 mm x 130.7 mm. Sliding minimum background subtraction was used to remove background image noise. LaVision DaVis 8.0 software was used to correlate vectors in multipass mode. Three passes were made with 128 x 128 window size with 87% overlap, and three passes with 64 x 64 window size with 87% overlap resulting in a 80 x 39 vector map for the given interrogation region.

Similar to the cylinder flow, the airfoil flow field possesses well-defined natural and controlled states. These are clearly shown in the flow visualization images shown in Figure 6. Figure 6d shows that natural flow state with the plasma off. The flow is clearly separated from the airfoil leading edge. Figure 6b shows the flow in the controlled state with the plasma on. The flow is now attached to the airfoil surface. Figure 6a shows a representative image of the transient state between natural and controlled flow shortly after initiation of the leading edge plasma. Figure 6c presents an image of the transient state between controlled and natural states after the leading edge plasma is extinguished. The experiment consisted of acquisition of 250 ensembles of the velocity field, each of 400 ms duration in which the plasma is initiated at $\tau = 0$ and extinguished at $\tau = 150$ms so that the duty cycle was 37.5%. Although there was considerable cycle-to-cycle variation, in general the transient state after plasma initiation was $\Delta\tau$

$\approx$ 40 ms duration. The controlled state occurs from approximately τ = 35 – 150 ms during which time the plasma maintains flow attachment. The plasma is extinguished at τ = 150 ms which initiates a second transient state of approximate duration of 150 ms in which the flow returns to the natural separated state. In this manner each ensemble contained a natural flow state of approximately 100 ms in duration.

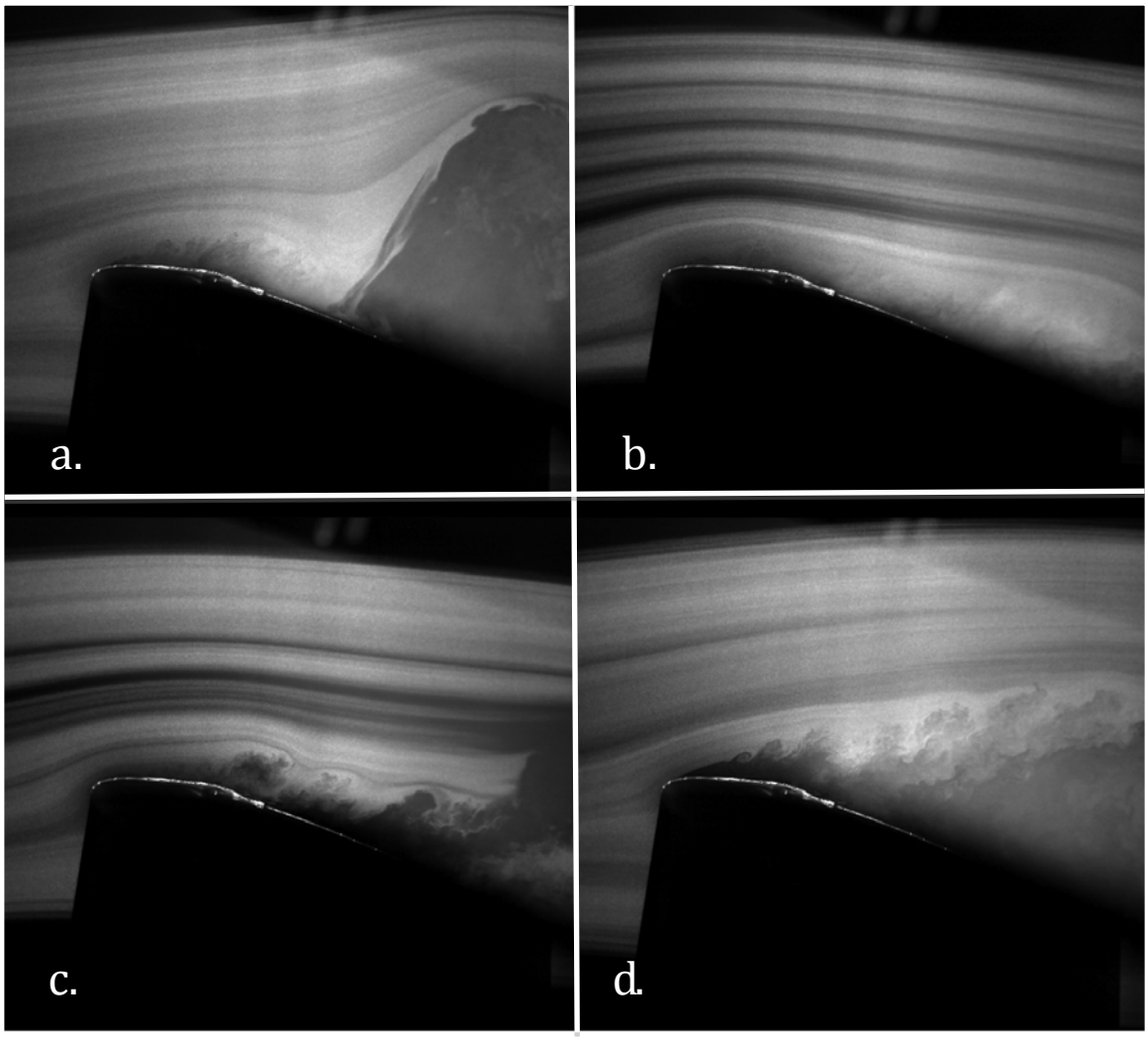

Figure 6: Visualization of the flow over the NACA 0015 airfoil at Re_c = 86,000: (a) Transition state 1 (plasma switched on), (b) Controlled state (attached flow), (c) Transition state 2 (plasma switched off), (d) Phase 4: Natural state (separated flow).

IV. Results

A. TPOD Modes for Cylinder Flow Control Experiment

The experimental 2-D velocity field was processed to extract time-dependent TPOD modes using the method of snapshots [17], as described before. The freestream velocity was subtracted from each velocity field. Figure 7 shows the spanwise vorticity associated with the first TPOD mode at several representative time delays, τ, from the actuation-on part of the cycle. The corresponding temporal evolution of energy for the first 5 TPOD modes is shown in Figure 8. Figure 8 shows that the first TPOD mode holds between 60% and 85% of the total resolved kinetic energy. It is apparent from examination of both figures 7 and 8 that the flow undergoes a rather drastic change as it switches between the natural and controlled states. This occurs between time delays of τ = 0 and approximately 50 ms as vortex shedding is eliminated. The plasma flow control is terminated at τ = 125 ms and the Figure 7, image at

τ = 141 ms, shows the renewal of vortex shedding while Figure 8 shows an increase in modal energy with τ once the plasma is extinguished. Clearly, the flow is phase-locked, so that shed vortices are seen in Figure 7 at τ = 179 and 221 ms, for instance.

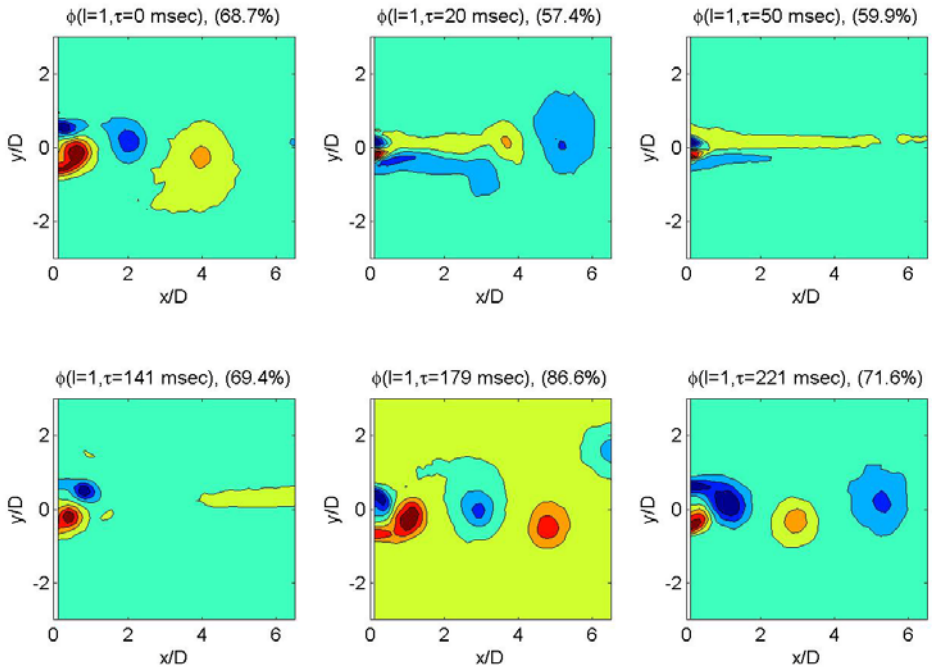

Figure 7. The vorticity associated with the first TPOD mode, $\varphi_1(x,y;\tau)$ at different representative time-delays. The actuation is turned on at τ = 0 msec and is turned off at τ = 125 msec. Phase shift is zero degrees. Numbers in parenthesis are the relative amounts of energy in TPOD mode 1; $\lambda_1(\tau)/\sum_i \lambda_i(\tau)$.

Knowing the TPOD modes at given discrete times, the first six spatial-only Ψ(i,j)-modes (Eq. 4) for the first TPOD mode, $\varphi_1(x,y;\tau)$, are presented in Figure 9, left plot. The first mode, Ψ(1,1), represents the mean natural flow. The fourth mode, Ψ(1,4), is a linear combination of the mean flows during the natural and forced states and is related to the "shift" mode [6]; the second and the third modes, Ψ(1,2) and Ψ(1,3), describe the vortex shedding behind the cylinder and higher modes are responsible for the transient regime between the natural and the controlled cases.

Temporal coefficients, *c*(i,j), (Eq. (4)) for these first six Ψ-modes for all eight phases which were calculated by projecting the first TPOD mode into the spatial Ψ-mode frame of reference and are shown in Figure 9, right plot. These coefficients represent the temporal evolution of the "most-energetic" portion of the flow from the given phase point on the natural cycle. As expected, the temporal evolution of second and the third Ψ-mode, which are responsible for the shedding cycle depend on the initial phase. The phase dependence of the temporal evolution of the first and the forth Ψ-modes is negligible, implying that the change in the mean flow does not depend on the phase of the shedding cycle. Finally, the fifth and the sixth Ψ-modes, which are responsible for the transient effects show a moderate dependence on the initial shedding phase.

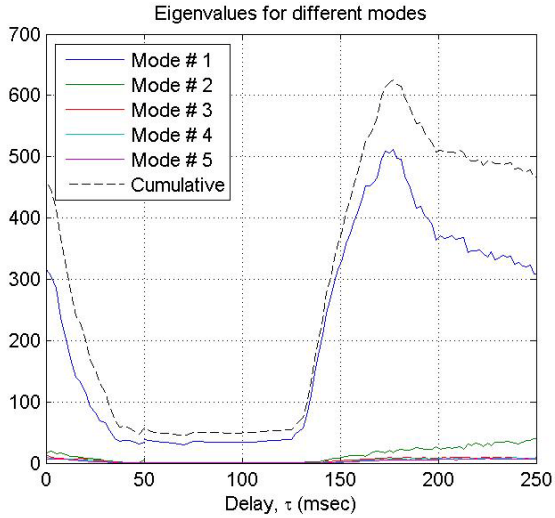

Figure 8. TPOD mode eigenvalues, $\lambda_i(\tau)$ and cumulative energy $\sum_i \lambda_i(\tau)$ at different time delays.

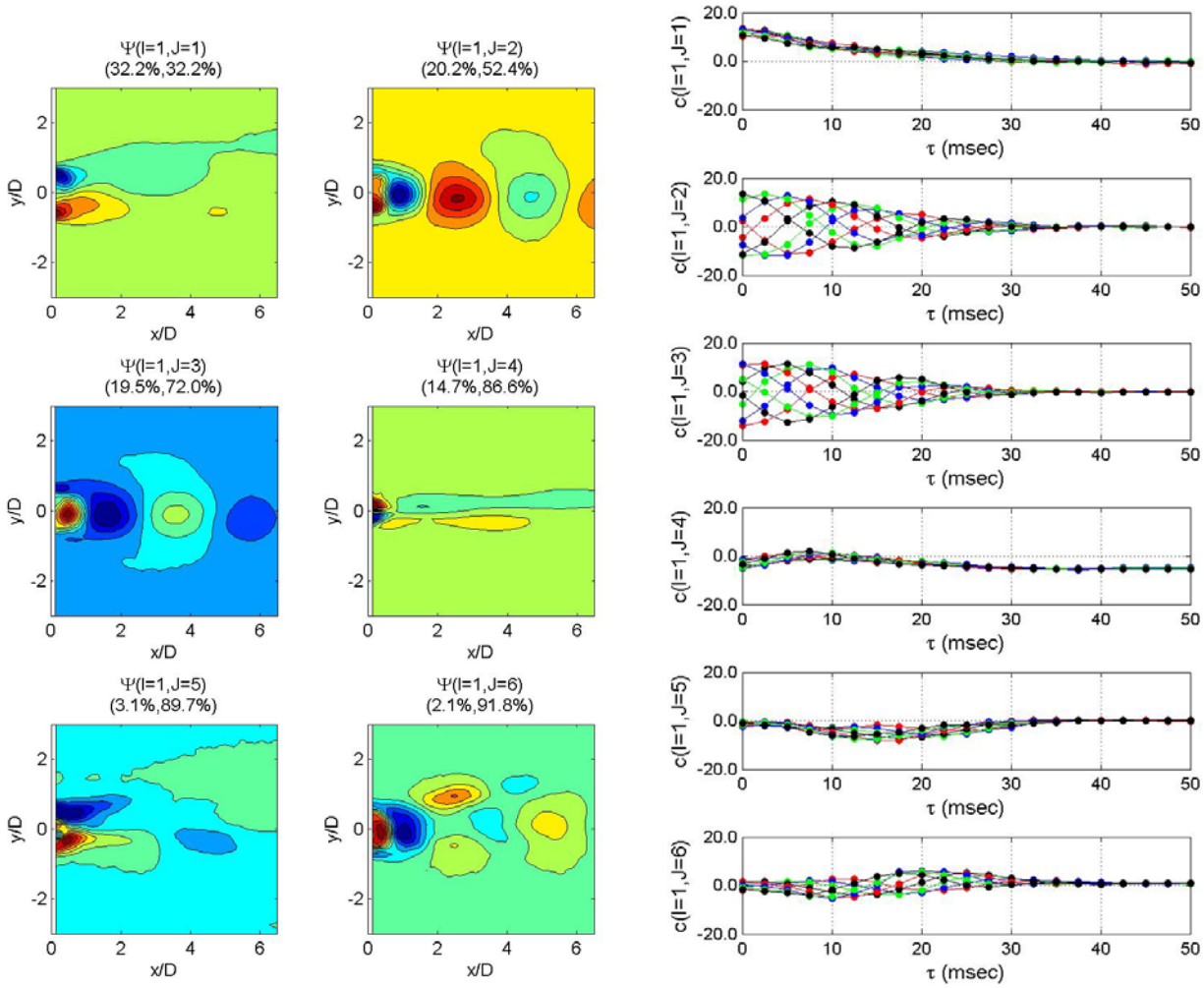

Figure 9. (Left) Modes Ψ(i,j) and (right) corresponding coefficients *c*(i,j), defined in Eq. (4) for eight different phases.

In order to check how well the velocity realizations were phase-locked at the moment the flow control was turned on, which corresponds to the delay time $\tau = 0$, all individual flow realizations for all phases were projected into the vortex shedding Ψ-modes, Ψ(1,2) and Ψ(1,3). The results are plotted in Figure 10. The two phases of 0 and 180 degrees are highlighted by blue and red dots, respectively. Also, the temporal coefficients of the first TPOD mode, $c(1,2)$ and $c(1,3)$, at $\tau = 0$ for these phases are presented as solid black circles in Figure 8. The system in the natural state clearly has a limiting cycle in this Ψ-mode space. Individual velocity realizations are relatively-highly clustered around the corresponding selected phase points, thus verifying the hot-wire-based conditional sampling technique.

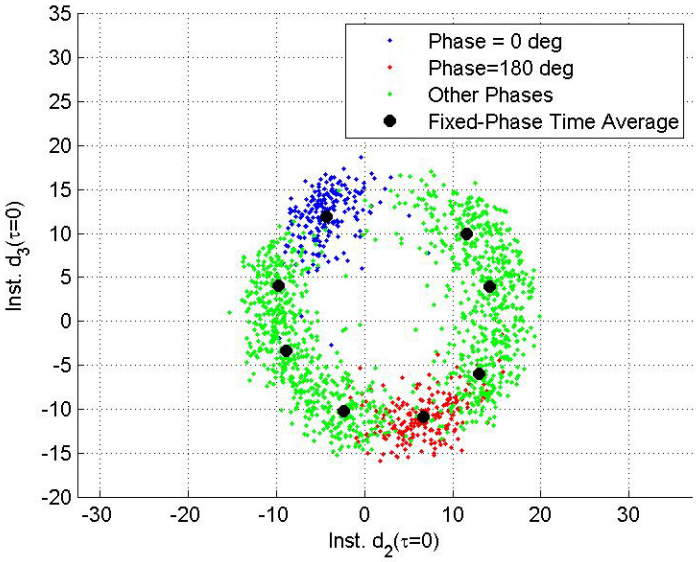

Figure 10. Projection of instantaneous velocity fields into Ψ(1,2) and Ψ(1,3), defined in Eq. (5) for different phases.

B. TPOD modes for Airfoil Flow Control Experiment

TPOD was also applied for the flow around the NACA 0015 airfoil at the post-stall angle of attack $\alpha = 18^o$ with the DBD plasma flow control applied at the leading edge, as described before. A total of 250 time-resolved PIV realizations were collected and analyzed. The mean flow in the natural state, $U^N(x,y) = E\{u(x,y,\tau=0,t_0 \in \{t_0\}_\alpha\}_\alpha$, was subtracted from each flow realization and the TPOD eigenmodes and the corresponding eigenvalues were computed as a function of the time delay, τ, using Eq.(1). The first two TPOD modes at time delays, τ = 10, 20, 30 and 50 msec are presented in Figure 11. The first TPOD mode primarily reflects the changes in the mean flow, while the second TPOD mode describes the evolution of the vortical structures during the transient regime. Eigenvalues for first four TPOD modes and the total amount of the energy at different time delays are presented in Figure 12, left plot and the relative amount of energy in the first four TPOD modes are shown in Figure 12, right plot. When the flow control is applied at $\tau = 0$ msec, the flow did not respond instantly to the flow control, as both the total and the modal energies were roughly constant during the first 15 ms. The flow subsequently started to respond to the flow control and transitioned to the control state for time delays between 15 and 40 ms; the cumulative energy and the energy of the first mode sharply increased in this time interval, as the flow control pushed the separation point toward the trailing edge and created a higher-speed, more energetic region near the airfoil suction surface, as seen in Figure 6b. The relative amount of energy in the first TPOD mode went from 40 to nearly 90 percent during this natural-to-control transient regime, while the second mode first went up to 30% of the total energy and then came down to only a few percent. All higher modes contributed less than 6 % during the transient regime. In the control state the total amount of energy was slightly fluctuating as the flow control did not completely re-attach the flow over the airfoil at this high post-stall angle of attack of 18^o. At τ = 150 ms, the flow actuation was turned off and the flow started to relax back to its natural state; this control-to-natural transient regime lasted approximately 150 ms.

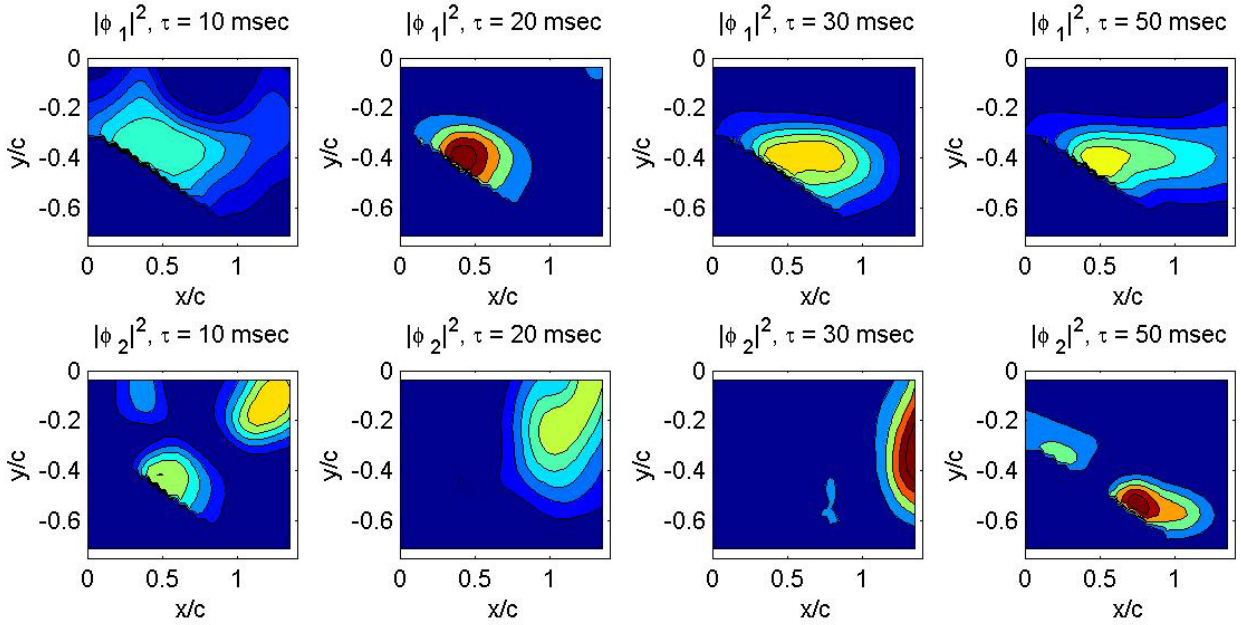

Figure 11. Square of the amplitude of the first and the second TPOD mode for selected time delays. Flow goes from left to right, the airfoil surface is present as a velocity discontinuity line.

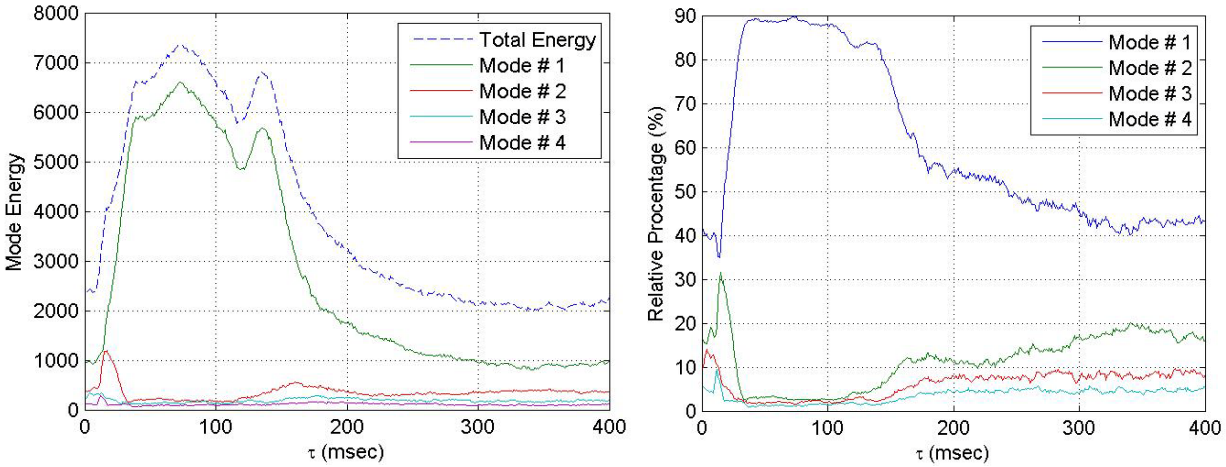

Figure 12. Left plot: First four TPOD mode eigenvalues, $\lambda_i(\tau)$ and cumulative energy $\sum_i \lambda_i(\tau)$ at different time delays. Right plot: Normalized eigenvalues $\lambda_i(\tau) / \sum_i \lambda_i(\tau)$ for the first four TPOD modes at different time delays.

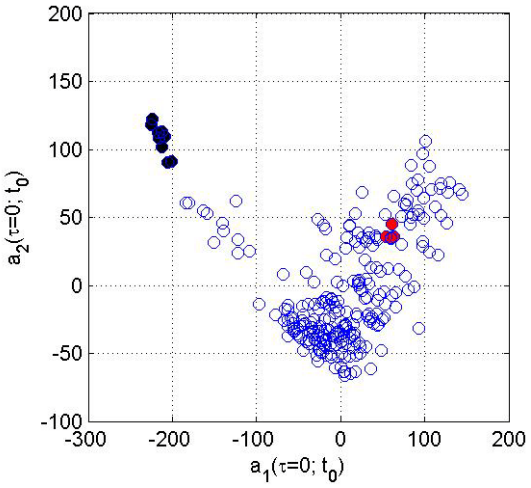

Figure 13. Values of temporal coefficients of the first and the second TPOD at $\tau = 0$. Two selected groups of initial conditions are labeled by black and red circles.

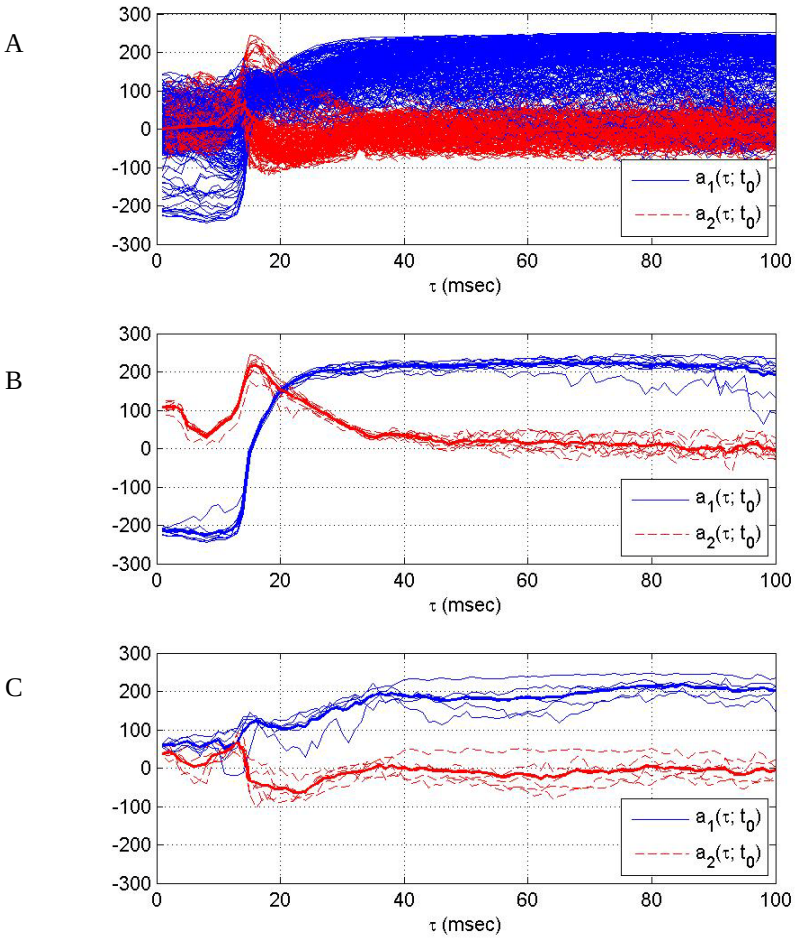

Figure 14. Temporal evolution of first two TPOD modes for (A) all trajectories, and trajectories originated from the two groups, labeled by (B) black and (C) red circles in Figure 13. Corresponding conditionally-averaged trajectories for both TPOD modes are plotted as thicker lines in plots B and C.

After the TPOD modes were calculated, temporal coefficients, defined in Eq. (3) were computed for each flow realization. Figure 13 shows all temporal coefficients for the first two TPOD modes at $\tau = 0$ msec, just before the flow control was activated. Unlike the flow around the cylinder, where initial points were contained on a simple limiting cycle (see Figure 10), all initial points for the airfoil flow in the natural state occupy a more complex region. The temporal evolution of the coefficients for the first two modes for all 250 flow trajectories are plotted in Figure F14A, revealing a complex set of different trajectories from the natural to the controlled state. To illustrate the ability of TPOD approach to extract conditional-averaged events, two distinct small subsets or regions of the initial conditions were arbitrarily selected. The first group, labeled by black circles in the far upper left corner in Figure 13, represents a statistically rare event in the flow. The second group of initial conditions is labeled by red circles in Figure 13 and represents a more typical transient event. Once the initial moments were selected, the temporal evolutions of the TPOD coefficients of the selected subsets were calculated, along with the subset-ensemble-averaged trajectories for both groups. The results for the first group are shown in Figure 13B. All trajectories exhibited some small variation around the ensemble-averaged trajectory. The first TPOD mode remains at a constant negative value of -200 for the first 15 ms, after which it quickly went to a positive value of approximately 200 between 15 and 30 ms and subsequently stayed constant after 30 ms. The second TPOD mode was essentially non-zero during the first 40 ms before leveling off at a zero-value. Trajectories in the second group shown in Figure 13C exhibit a larger spread from the conditionally-averaged trajectory. The transient process was slower for the this group of trajectories, with both modes leveling off at approximately $\tau =$ 40 ms after the flow control was activated.

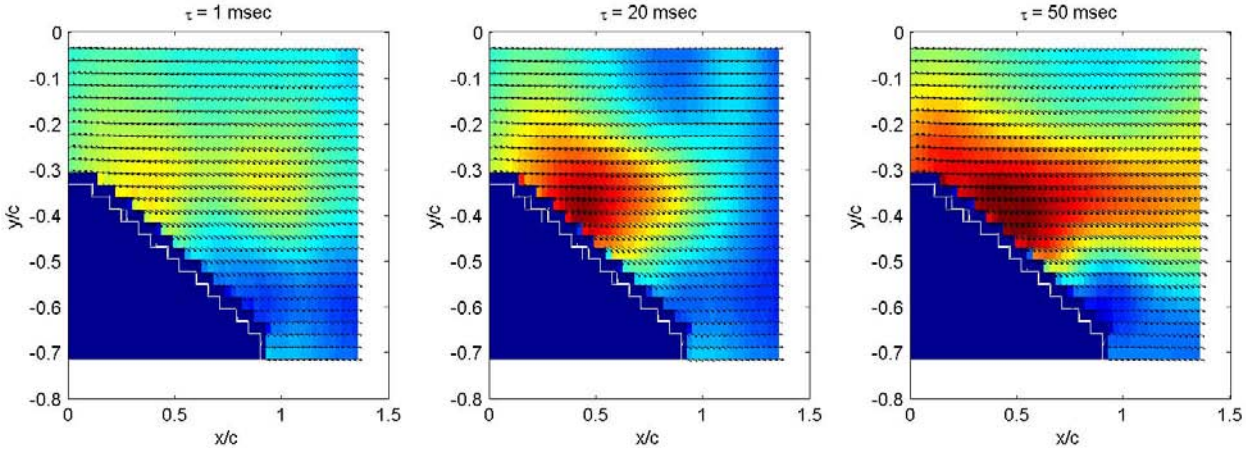

Figure 15. Reconstructed velocity field (velocity vectors and square of the amplitude) using first two TPOD modes using conditionally-averaged trajectories from Figure 14B.

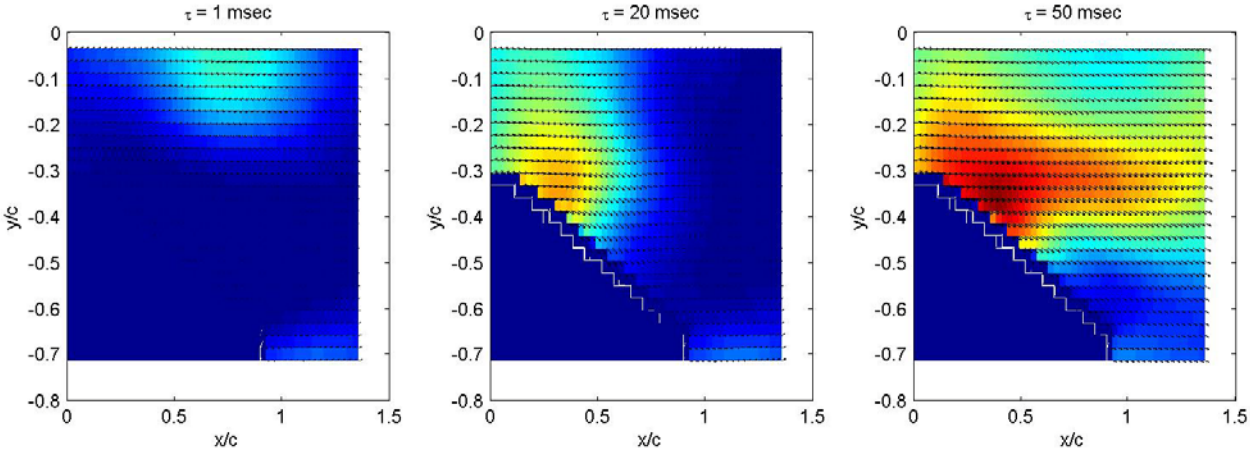

Figure 16. Reconstructed velocity field (velocity vectors and square of the amplitude) using first two TPOD modes using conditionally-averaged trajectories from Figure 14C.

Using conditionally-averaged trajectories of the first two TPOD modes, corresponding instantaneous velocity fields for conditional-averaged trajectories for both groups were re-created as, $u(x,y;\tau) \approx U^N(x,y) + \sum_{i=1}^{2} E\{a_i(\tau,t_0)\}_{SubSet-of-t_0} \varphi_i(x,y;\tau),$. Results for the first group at τ = 1, 20 and 50 ms are given in Figure 15 and the results for the second group are plotted in Figure 16. Inspection of the reconstructed velocity field for the first group (the statistically rare event) revealed that the flow remained partially attached before the flow control was activated and therefore it quickly became fully attached over the suction side of the airfoil when the flow control was activated. In contrast, results of the velocity reconstruction for the trajectories in the (more common) second group showed that the flow was fully separated before the flow control was activated and as a consequence it took the flow a longer period of 40 ms to go to the control state. In both cases, with plasma flow control applied at the leading edge, flow attachment is not maintained to the airfoil trailing edge due to the high angle of attack of the airfoil.

Conclusions

This paper has demonstrated the ability of TPOD to extract the optimum set of eigenmodes and their temporal evolution in two separate active flow control experiments: (1) plasma flow control of vortex shedding from a circular cylinder in cross-flow and (2) leading edge plasma separation control of a NACA 0015 airfoil at a large post-stall attack angle. In both cases, the TPOD method is shown to provide the ability to optimally characterize not only the distinct natural and controlled flow states, but also the transient system trajectories between these states. This ability comes as a consequence of retaining time in the TPOD spatial-temporal modes. In both experiments it is demonstrated that the TPOD approach provides the unique ability to conditionally examine families of flow trajectories between natural and controlled states for user selected initial conditions, t_o. This can be extremely useful in order to understand the physical mechanisms of flow control in complex flows where there may be very little apriori knowledge of the system behavior. Also, unlike conditional-sampling experiments, where the conditional event is defined and the system evolution is studied *after* the conditional event, the knowledge of flow trajectories in space and time allows to study the system evolution *before and after* the conditional event. It is extremely useful for flow control applications, if, for example, a conditional event is defined after the flow control is applied and trajectories can be traced back in time to find out which subset of the initial times would lead to the desired event in the future.

Although not explored in this paper, the TPOD modes also provide a very efficient framework for the development of low-order models capable capturing the dynamics of the natural, controlled and transient states of the flow, as well as hysteresis effects with the presence of the flow control. This will be one focus of our future work.

Acknowledgments

The authors would like to acknowledge the financial support of NASA through Cooperative Agreement NNX07AO09A. The time-resolved PIV system was acquired under DURIP award W911NF-10-1-0164 administered through the Army Research Office. This support is also gratefully acknowledged.

References

[1]Berkooz, G., Holmes, P., & Lumley, J. L. 1993, "The proper orthogonal decomposition in the analysis of turbulent flows," *Ann. Rev. Fluid Mech*., **25**, 539-575.

[2]Holmes, P., Lumley, J. L., & Berkooz, G., 1996, *Turbulence, Coherent Structures, Dynamical Systems and Symmetry*, Cambridge University Press.

[3]Lumley, J., 1970, *Stochastic Tools in Turbulence*, Academic, New York.

[4]Aubry, N., Holmes, P., Lumley, J. L., & Stone, E., 1988, "The dynamics of coherent structures in the wall region of the turbulent shear layer," *J. Fluid Mech.* **192**, 115-175.

[5]Ukeiley, L. S., Cordier, L., Manceau, R., Delville, J., Glauser, M. N., & Bonnet, J.P., 2001, "Examination of large-scale structures in a turbulent plane mixing layer. Part 2. Dynamical systems model," *J. Fluid Mech.*, **441**, 67-108.

[6]Siegel, S. G., Seidel, J., Fagley, C., Luchtenburg, D. M. & McLaughlin, T., 2008, "Low-dimensional modeling of a transient cylinder wake using double proper orthogonal decomposition," *J. Fluid Mech.*, **610**, 1-42.

[7]Siegel, S. G., Cohen, K., Seidel, J., Aradag, S., and McLaughlin, T. "Low Dimensional Model Development using Double Proper Orthogonal Decomposition and System Identification", 4th Flow Control Conference, June, 2008, AIAA-2008-4193.

[8]R. C. Camphouse, J. H. Myatt, R. F. Schmidt, M. N. Glauser, J. M. Ausseur, M.Y. Andino, and R. D. Wallace, "A Snapshot Decomposition Method for Reduced Order Modeling and Boundary Feedback Control", *Paper AIAA-2008-4195*, 4th Flow Control Conference, Seattle, Washington, 2008.
[9]Rowley, C. W., 2005, "Model reduction for fluids using balanced proper orthogonal decomposition", *Int. J. Bifurcation Chaos* **15** (3), 997–1013.
[10]Juang, J.N., Pappa, R.S." An eigensystem realization algorithm for modal parameter identication and model reduction," *J. Guid. Contr. Dyn*. **8**(5), 620-627, 1985.
[11]Z. Ma, S. Ahuja, and C. W. Rowley ,"Reduced order models for control of fluids using the Eigensystem Realization Algorithm", *Theoret. Comput. Fluid Dyn.* (online), February 2010.
[12]Gordeyev, S. and Thomas, F. O., "A Temporal Proper Orthogonal Decomposition (TPOD) Method for Closed-Loop Flow Control," AIAA paper 2010-0359, 48th Aerospace Sciences Meeting, Orlando, FL, 4-7 January 2010.
[13]Kozlov, A. V. and Thomas, F. O., "Control of Bluff Body Flow via Two Types of Dielectric Barrier Discharge Plasma Actuation," *AIAA J*., in press, 2011.
[14]Corke, T. C., Post, M. L., Orlov, D. M., "Single Dielectric Barrier Discharge Plasma Enhanced Aerodynamics: Physics, Modeling and Application," Exp. Fluids, 46, 2009, pp. 1-26.
[15]Moreau, E., "Airflow Control by Non-Thermal Plasma Actuators," *J. Phys D Appl Physics*, 40, pp. 605-636
[16]Thomas, F. O., Corke, T. C., Iqbal, M., Kozlov, A., and Schatzman, D., "Optimization of SDBD Plasma Actuators for Aerodynamic Flow Control," *AIAA Journal*, 47,9, 2009, pp. 2169-2178.
[17]Sirovich ,L, 'Turbulence and the Dynamics of Coherent Structure: I, II and III', *Quarterly Applied Mathematics*, (1987), **45**, p. 561.